Generation of electron vortex beams using line charges *via* the electrostatic Aharonov-Bohm effect

Giulio Pozzi [a,b,*], Peng-Han Lu [b], Amir H. Tavabi [b], Martial Duchamp [b,1], Rafal E. Dunin-Borkowski [b]

[a] *Department of Physics and Astronomy, University of Bologna, Viale B. Pichat 6/2, 40127 Bologna, Italy*
[b] *Ernst Ruska-Centre for Microscopy and Spectroscopy with Electrons and Peter Grünberg Institute, Forschungszentrum Jülich, 52425 Jülich, Germany*

A B S T R A C T

It has recently been shown that an electron vortex beam can be generated by the magnetic field surrounding the tip of a dipole-like magnet. This approach can be described using the magnetic Aharonov-Bohm effect and is associated with the fact that the end of a long magnetic rod can be treated approximately as a magnetic monopole. However, it is difficult to vary the magnetisation of the rod in such a setup and the electron beam vorticity is fixed for a given tip shape. Here, we show how a similar behaviour, which has the advantage of easy tuneability, can be achieved by making use of the electrostatic Aharonov-Bohm effect associated with an electrostatic dipole line. We highlight the analogies between the magnetic and electrostatic cases and use simulations of in-focus, Fresnel and Fraunhofer images to show that a device based on two parallel, oppositely charged lines that each have a constant charge density can be used to generate a tuneable electron vortex beam. We assess the effect of using a dipole line that has a finite length and show that if the charge densities on the two lines are different then an additional biprism-like effect is superimposed on the electron-optical phase.

1. Introduction

The term vortex beam (VB) describes freely propagating particles that have a helical wavefront and carry an amount of orbital angular momentum (OAM) about their axis of propagation that is non-zero and may be quantised. In light optics, VBs are now used in many applications, such as optical tweezers and spanners for nano-manipulation, phase contrast imaging and both classical and quantum communication (*e.g.*, [1]). It is expected that similar success can be achieved in electron microscopy, where an electron VB (EVB) could be used to investigate magnetic properties of materials at the atomic or near-atomic scale, to manipulate nanoparticles or to measure electron-optical parameters (see, *e.g.*, the reviews of [2,3]). In analogy to light optics [4–6], it is envisaged that the use of a spiral phase plate could also be used to improve the contrast of weakly scattering biological specimens [7].

EVBs can be generated by using a thin film of suitably varying thickness that imprints on the electron beam a spirally increasing phase front [8], a holographic fork aperture [9,10], a holographic spiral aperture [11,12], a hardware aberration corrector [13] or the magnetic field surrounding the sharp tip of a dipole-like magnet [7,14]. The latter approach is based on the magnetic Aharonov-Bohm effect [15] and relies on the fact that the end of a long magnetic rod can be described approximately as a magnetic monopole. However, it is not straightforward to vary the magnetisation of such a rod once it has been fabricated. The device therefore suffers from limited tuneability for altering the vorticity of the EVB.

This drawback can be overcome by using the electrostatic counterpart of the Aharonov-Bohm effect [16–20] and specifically by using the electrostatic field at the end of a long dipole to create an electrostatic monopole field. Such a device can be approximated experimentally by covering one side of a metallic wire with a different metal so that the contact potential difference creates a dipole field [16,17], or alternatively by using a rod coated with a material such as ZnO followed by the angled evaporation of a metal such as Au [21]. However, in both of these arrangements the phase shift can only be varied by rotating the wire or rod, also resulting in limited tuneability.

---

* Corresponding author.
E-mail address: giulio.pozzi@unibo.it (G. Pozzi).
[1] Present address: School of Materials Science and Engineering, Nanyang Technological University, 50 Nanyang Avenue, Singapore 639798

Here, we propose to create an electrostatic monopole field by using two thin metallic parallel wires, to which an external voltage source is used to apply a potential difference. Such an arrangement is difficult to realise experimentally, but is highly versatile because the potential difference applied to the wires can be varied at will, limited only by the possibility of an electrical discharge between the wires.

After reviewing the basic analogies between the magnetic and electrostatic Aharonov-Bohm effects, we introduce the system of two parallel lines that carry opposite but constant charge density distributions. We show that the two wires constitute an electrostatic analogue of a uniformly-magnetised bar. Based on our previous experience in the study of caustics arising from electrostatic fields between two nearly-aligned tips that were subjected to opposite potentials [22], we suggest that such a device can be fabricated from two suitably-shaped metallic wires, whose surfaces coincide with desired equipotential surfaces at a chosen distance from the line charges. We argue that two rounded parallel metallic wires should provide a good approximation to the ideal case. The influence of the lengths of the wires and the charge distributions on them on Fresnel and Fraunhofer diffraction patterns are presented and discussed.

2. Theoretical considerations

The electrostatic scalar potential associated with an elementary dipole of moment $\mathbf{p} = q\delta\mathbf{l} = (p_x, p_y, p_z)$ is given by the expression [23]

$$V(x, y, z) = \frac{1}{4\pi\epsilon_0} \frac{\mathbf{p} \cdot \mathbf{R}}{R^3}, \qquad (1)$$

where $\mathbf{R} = (x, y, z)$.

According to the high energy or phase object approximation [20,24], a weak electromagnetic field can be approximated (in the gauge div $\mathbf{A} = \mathbf{0}$) by a thin specimen, which is located at the position of the field sources (*e.g.*, metallic wires or magnetic needles) in the electron beam direction and characterised by a two-dimensional transmission function of the form

$$A(x, y) \exp(i\varphi(x, y)), \qquad (2)$$

where the amplitude $A(x, y)$ is zero in the shadows of the supports if they are opaque to electrons.

The electron-optical phase shift $\varphi(x, y)$ can be written in the form

$$\varphi(x, y) = \frac{\pi}{\lambda E} \int_z V(x, y, z)dz - \frac{e}{\hbar} \int_z A_z(x, y, z)dz, \qquad (3)$$

where the incident electron beam direction z is aligned with the optical axis, e is the absolute value of the electron charge, $\hbar$ is the reduced Planck constant, λ is the relativistically corrected de Broglie electron wavelength, eE is the relativistically corrected electron energy and $A_z(x, y, z)$ is the z component of the magnetic vector potential (not to be confused with the amplitude $A(x, y)$). The integral is extended along the z axis, with integration limits that include all of the field.

It follows from Eqs. 1 and 2 that for an electrostatic dipole

$$\varphi_e(\mathbf{r}) = \frac{\pi}{\lambda E} \frac{1}{2\pi\epsilon_0} \frac{p_x x + p_y y}{x^2 + y^2}. \qquad (4)$$

Direct integration can then be used to evaluate the phase shift associated with a continuous distribution of electric dipoles that are aligned along x (*i.e.*, $p_y = 0$) and distributed uniformly along the y axis between $-a$ and a with constant density n_{el}, resulting in the expression

$$\varphi_{ld}(\mathbf{r}) = \frac{\pi}{\lambda E} \frac{1}{2\pi\epsilon_0} p_x n_{el} \left[\arctan\left(\frac{a - y}{x}\right) + \arctan\left(\frac{a + y}{x}\right) \right]. \qquad (5)$$
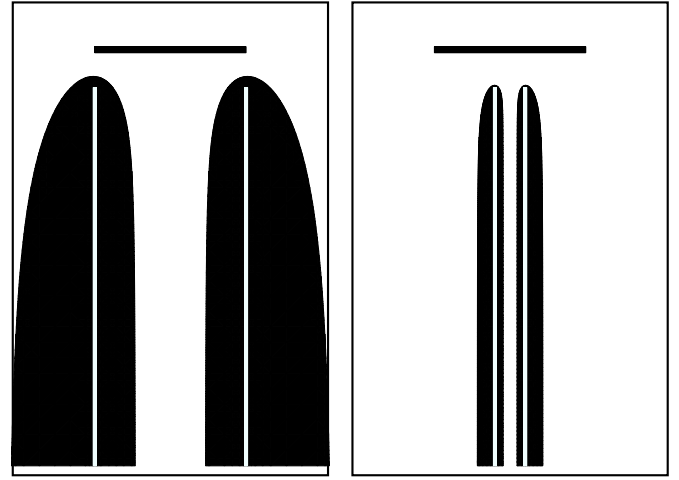
Fig. 1. Line charges of length 100 μm and separation 200 nm (white lines) with constant charge densities of $C_V = 1$. The overlaid amplitude images (black outlines) show corresponding ± 2 V potential surfaces. The left image (scale bar 200 nm) shows the region around the tips. The right image shows a wider area (scale bar 1 μm).

In the limit $a \to \infty$:

$$\varphi_{ld}(\mathbf{r}) = \frac{\pi}{\lambda E} \frac{p_x n_{el}}{2\epsilon_0} \text{sign}(x), \qquad (6)$$

which describes a constant phase difference that depends on electron energy eE and wavelength λ, as well as on the orientation of the dipoles.

A similar calculation of the phase shift for a magnetic flux tube, which carries magnetic flux Φ, has finite length and is aligned along the y direction [20,23,25], results in the expression

$$\varphi_{ft}(\mathbf{r}) = \frac{e}{\hbar} \frac{\Phi}{2\pi} \left[\arctan\left(\frac{a - y}{x}\right) + \arctan\left(\frac{a + y}{x}\right) \right]. \qquad (7)$$

For an infinite flux tube:

$$\varphi_{ft}(\mathbf{r}) = \frac{e}{\hbar} \frac{\Phi}{2} \text{sign}(x), \qquad (8)$$

which describes a phase difference that is independent of electron energy and wavelength and equal to that calculated by Aharonov and Bohm [15].

The formal identity between the electrostatic and magnetic cases shows that the phase shift of a line of electrostatic dipoles is equivalent to that of a magnetic flux tube. The phase distribution at the end of an electric dipole line can therefore be considered to be the electrostatic analogue of the phase distribution of a magnetic monopole at the end of a magnetic flux tube.

We emphasise that the magnetic flux tube and the line of electrostatic dipoles are both limiting cases that cannot be realised perfectly in practice. In the magnetic case, the closest approach is represented by a magnetic slab of width $2w$, which can be described by integrating Eq. 7 along x between $-w$ and w [26]. The result is a complicated analytical expression that is reported in [27]. A similar calculation carried out for the electrostatic case using Eq. 5 leads to the conclusion that the phase shift is equivalent to that of two oppositely charged segments, which are separated by w, have a constant charge density along each of them and therefore represent the electrostatic analog of the magnetic bar.

3. The electrostatic field of two charged segments

In a recent study of caustics [22], we obtained an analytical expression for the electrostatic potential and the electron-optical
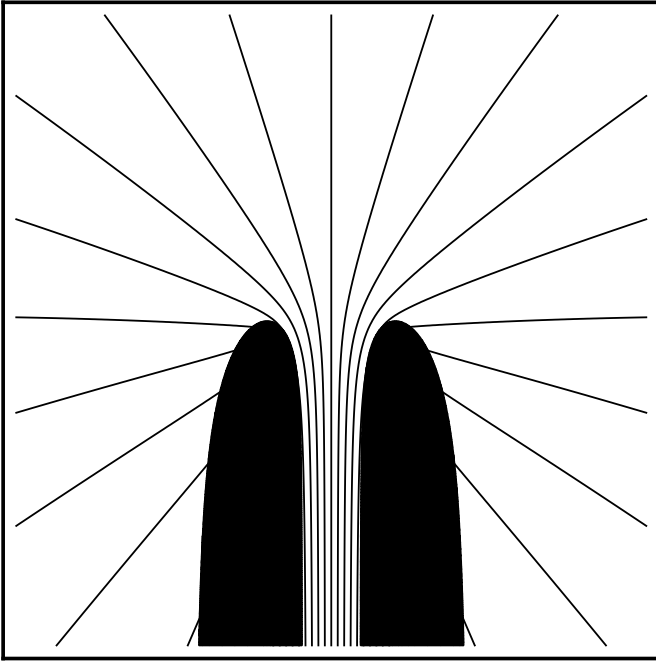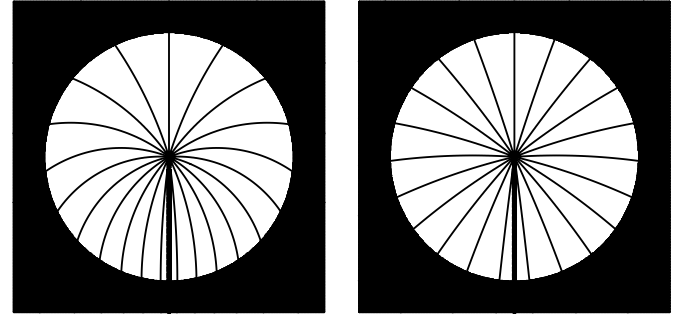
Fig. 2. Equiphase lines of spacing $\pi/4$ radians and overlaid amplitude image, shown for a 1 μm × 1 μm field of view, a wire length of 100 μm and a wire separation of 200 nm.

Fig. 3. Equiphase lines of spacing $\pi/4$ radians and overlaid amplitude image, shown for a 25 μm × 25 μm field of view. The left image corresponds to line charges of length 20 μm. The right image corresponds to line charges of length 100 μm. A beam-limiting aperture of diameter 20 μm is also shown.

phase shift of a line charge of constant charge density K, which lies in the $z = 0$ plane from $(0, -a)$ to $(0, 0)$ and is compensated by a neutralising charge in the same plane at (x_D, y_D). The neutralising charge in this simple model can be thought of as being located on a nearby conductor, which may be the side of the specimen holder or the wall of the microscope. As the neutralising charge is far from the end of the wire of interest, its influence on the potential can be neglected and the potential of the grounded conductor can be taken as 0 V.

The electrostatic potential in the $z = 0$ plane and the associated electron-optical phase shift, respectively, are given by the expressions

$$V(x, y, 0) = C_V \left[\log \left(\frac{\sqrt{(a+y)^2 + x^2} + a + y}{\sqrt{x^2 + y^2} + y} \right) - \frac{a}{\sqrt{(x+x_D)^2 + (y+y_D)^2}} \right] \quad (9)$$

and

$$\varphi(x, y) = C_E C_V \left[-(a+y) \log \left((a+y)^2 + x^2 \right) \right.$$
$$+ y \log \left(x^2 + y^2 \right) + 2a + 2x \tan^{-1} \left(\frac{y}{x} \right)$$
$$- 2x \tan^{-1} \left(\frac{a+y}{x} \right) + a \log \left((x+x_D)^2 \right.$$
$$\left. \left. + (y+y_D)^2 \right) \right], \quad (10)$$

where

$$C_V = \frac{K}{4\pi\epsilon_0} \quad (11)$$

and the interaction constant

$$C_E = \frac{\pi}{\lambda E}. \quad (12)$$

In particular, by taking two parallel line charges of equal length and opposite sign (*i.e.*, the electrostatic analog of the magnetic bar), the total charge is zero and there is no longer a need to introduce neutralising charges at large distances from the region of interest. Although line charges are an idealisation, their field can be reproduced exactly if two symmetric concave equipotential surfaces around the lines are filled with a metallic material, biased at opposite potentials and completely opaque to electrons [28].

Figure 1 shows the amplitude $A(x, y)$ of the transmission function, calculated in the high energy or phase object approximation, for two parallel charged lines, which are 20 μm in length and 200 nm apart and oppositely biased by an external voltage source. By plotting equipotential surfaces in the object plane (*i.e.*, in the plane of the charged lines) using Eq. 9 with $C_V = 1$, values of potential corresponding to the shapes of the two wires were chosen. In Fig. 1, the potentials are taken to be ± 2 V. By considering the
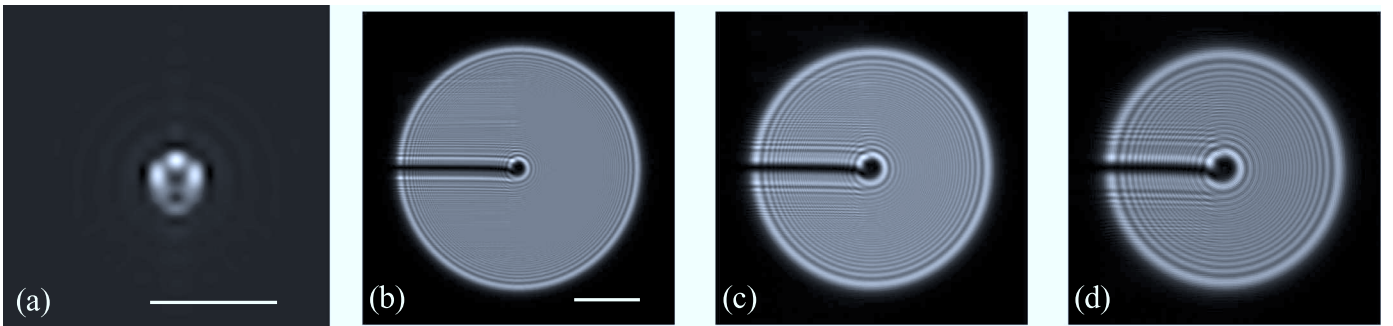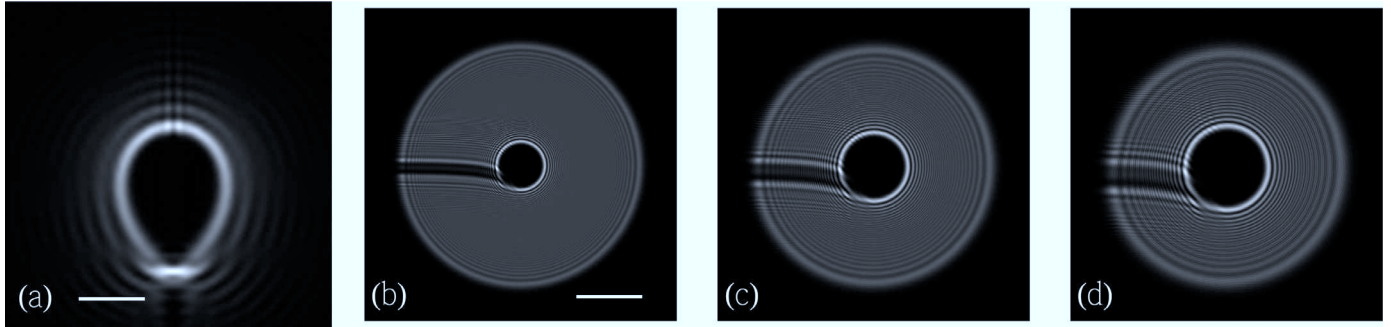

Fig. 4. Simulated images generated for line charges of length 100 μm and a potential difference of 4 V. (a) Fraunhofer diffraction image (scale bar 0.5 μm^{-1}). (b) - (d) show Fresnel images (scale bar 5 μm) for defocus values Z of 2, 4 and 6 cm, respectively.
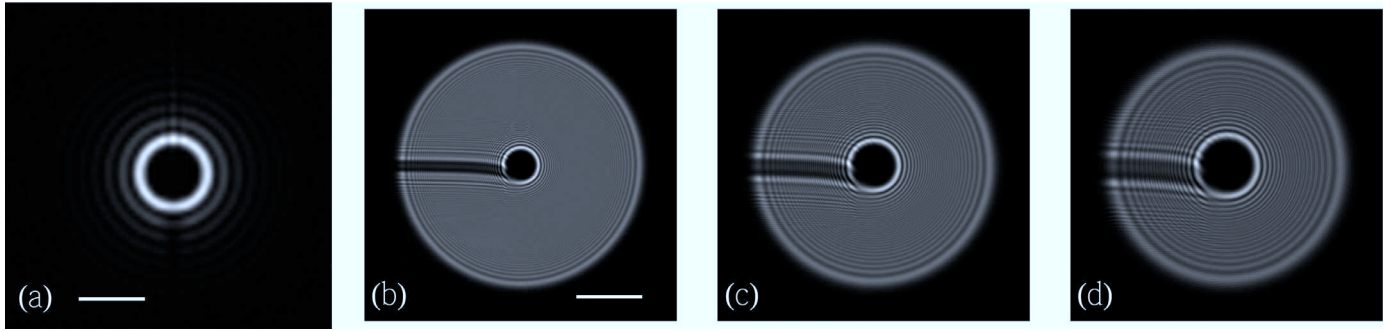
Fig. 5. Simulated images generated for line charges of length 100 μm and a potential difference of 20 V. (a) Fraunhofer diffraction image (scale bar 0.5 μm^{-1}). (b) - (d) show Fresnel images (scale bar 5 μm) for defocus values Z of 2, 4 and 6 cm, respectively.
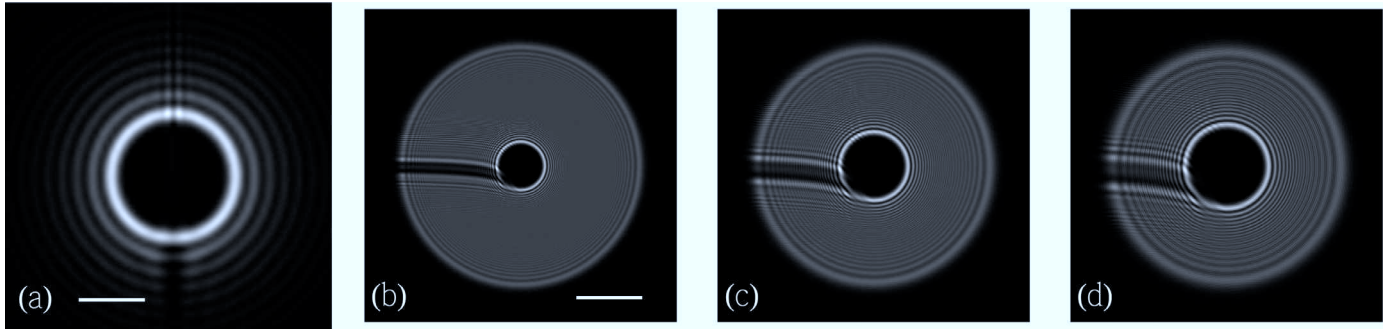
Fig. 6. Simulated images generated for line charges of length 100 μm and a potential difference of 40 V. (a) Fraunhofer diffraction image (scale bar 0.5 μm^{-1}). (b) - (d) show Fresnel images (scale bar 5 μm) for defocus values Z of 2, 4 and 6 cm, respectively.

Fig. 7. Simulated images generated for line charges of length 20 μm and a potential difference of 40 V. (a) Fraunhofer diffraction image (scale bar 0.5 μm^{-1}). (b) - (d) show Fresnel images (scale bar 5 μm) for defocus values Z of 2, 4 and 6 cm, respectively.

wires to be opaque to electrons, the amplitude $A(x, y)$ was chosen to be zero for values of potential inside the wires and unity outside. The left part of Fig. 1 shows the amplitude locally around the tips of the wires (scale bar 200 nm), while the right part shows a wider area (scale bar 1 μm). The white lines within the shadows mark the positions of the line charges. The shapes are the same for charged lines that are longer than 20 μm.

The phase shift was calculated for 300 kV electrons using Eq. 10. The resulting equiphase lines are shown in Fig. 2 with a spacing of $\pi/4$, alongside the amplitude, for a square field of view of side 1 μm. Figure 3 shows the equiphase lines and amplitude over a much larger area, together with an aperture of size 20 μm. In practice, such a metallic aperture should be placed in a plane conjugate to that of the wires in order not to perturb their fields. The left part of Fig. 3 corresponds to a charged line of length 20 μm and the right part to a charged line of length 100 μm. The opposite electrostatic monopole results in bending of the equiphase lines, which is more evident for the charged line of length 20 μm (left) than for that of length 100 μm (right). For a potential dif-

ference of 4 V, the phase difference is 5.2 π, corresponding to an orbital angular momentum of 2.6. For the same wire shape, larger values of potential difference can be obtained by varying the value of C_V.

It should be noted that the shapes of the wires are very important, in order to approximate the desired electrostatic configuration. For example, for charged perfectly cylindrical wires there is predicted to be an accumulation of charge at the tips, which may negatively affect the desired spiralling phase shift [29].

4. Results of simulations

Defocused images formed by illuminating a specimen using a coherent electron beam were simulated (in the paraxial approximation) by calculating the image wavefunction in the observation plane (X, Y, Z), where Z is the distance from the specimen plane, using the Kirchhoff-Fresnel integral [30]

$$\psi(X, Y, Z) = \frac{\exp(i\beta)}{\lambda Z} \iint A(x, y) \exp\left\{ \frac{i\pi}{\lambda Z}[(x - X)^2 \right.$$

$$+(y-Y)^2+\varphi(x,y)]\Big\}dxdy, \tag{13}$$

where λ is the de Broglie wavelength of the incident electrons and β is a phase factor that is unimportant here as only the intensity in the image plane, which is proportional to $|\psi|^2$, is relevant. Plane wave illumination was assumed.

We evaluated the Kirchhoff-Fresnel integral using a Fourier-transform-based method for square regions of side 25 μm using 1024×1024 sampling points. In the first step, a Fourier transform was used to calculate the spectrum of the image, which corresponds to the Fraunhofer diffraction image of the specimen. The spectrum was multiplied by a suitable quadratic phase factor [20,31]. An inverse Fourier transform was used to obtain the amplitude of the defocused image, while its modulus squared provided the image intensity.

Figure 4 shows the result of this procedure for a charged line of length 100 μm and a potential difference of 4 V. Figure 4 (a) shows a Fraunhofer diffraction image, *i.e.*, the spatial frequency spectrum. Corresponding Fresnel diffraction images of the specimen at defocus values of 2, 4 and 6 cm are shown in Figs 4 (b), 4 (c) and 4 (d), respectively. It should be noted that the Fraunhofer diffraction image does not display a clear dark area at its centre, as is typically observed for vortex beams. It is probably absent here due to the combined effects of diffraction from the shadow of the wires and the finite width between them. In contrast, the Fresnel diffraction images clearly show dark areas at their centres, with radii that increase with defocus.

We now investigate the effect on the images of the potential difference between the wires. Figure 5 shows results obtained for a potential difference of 20 V, which corresponds to an orbital angular momentum close to 13, whereas Fig. 6 shows results obtained for a potential difference of 40 V, which corresponds to an orbital angular momentum close to 26. Both figures show that the Fraunhofer diffraction image now has a clear intensity minimum at its centre and circular symmetry, with a radius that increases with applied potential difference. The Fresnel diffraction images also show impressive contrast phenomena surrounding the center of the electrostatic monopole.

In Fig. 3, we showed that the length of the charged lines has a strong influence on the phase, especially when the opposite monopole begins to influence the region of interest. Figure 7 shows the effect on the resulting Fraunhofer and Fresnel diffraction images for a potential difference between the wires of 40 V and for a wire length of 20 μm. (The effect is most visible at higher values of potential difference). The main effect of the reduction in length is seen in the Fraunhofer diffraction image shown in Fig. 7 (a), which is now strongly deformed and no longer has circular symmetry. In contrast, it is hardly detectable in the Fresnel diffraction images shown in Figs 7 (b-d).

More severe effects are seen in the Fraunhofer and Fresnel diffraction images when the two wires are not at opposite potentials, but an additional positive (or negative) potential is added to both of them. The physical origin of such an effect could be attributed to electron-beam-induced charging of dielectric material used to support the wires (in case they are not rigid enough), or alternatively to charging of the wires themselves.

Figure 8 shows results obtained for a defocus Z of 4 cm when adding potentials of (a, b) 0 V, (c, d) 0.01 V, (e, f) 0.05 V and (g, h) 0.1 V. Just as in Fig. 7, the most dramatic effects are seen in the Fraunhofer diffraction images, where the original circular intensity distribution is first deformed and finally broken. This effect is probably due to the breaking of the circular-spiral symmetry by the added line charge. In the corresponding Fresnel diffraction images, only a slight deformation of the central circular feature is seen and a weak convergent biprism-like effect appears along the
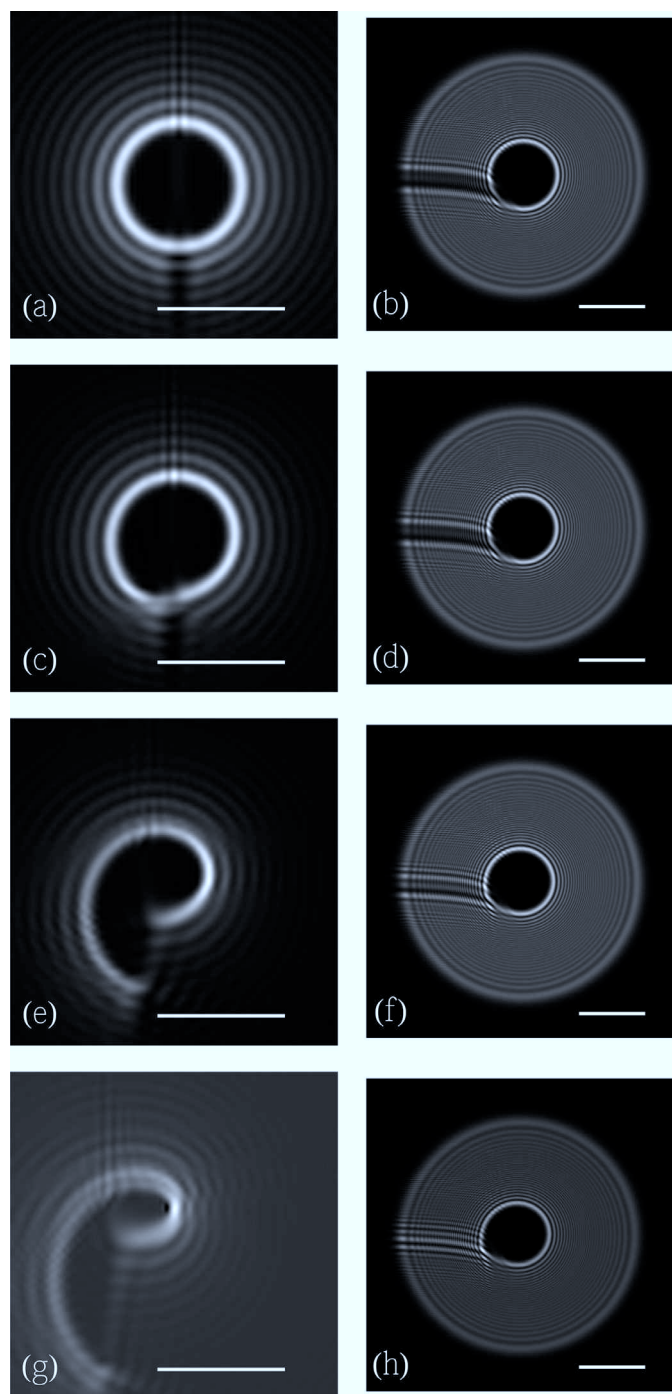
Fig. 8. Simulated Fraunhofer images (left) and Fresnel images (right) generated for line charges of length 100 μm, a potential difference of 40 V and added potentials of (a, b) 0 V, (c, d) 0.01 V, (e, f) 0.05 V and (g, h) 0.1 V. The Fresnel images were calculated for a defocus value Z of 4 cm. The scale bar in the diffraction images (a, c, e, g) is 0.5 $\mu\mathrm{m}^{-1}$. The scale bar in the Fresnel images (b, d, f, h) is 5 μm.

diffraction image of the wires. This effect is most evident for the largest added potential.

In spite of the very large fields between the wires, which are on the order of several tens of MV/m, we are well below the limits for field emission [32] and of electrical breakdown in small gaps [33], as also demonstrated by preliminary experimental tests.

5. Conclusions

In this paper, we have demonstrated that the electrostatic Aharonov-Bohm effect associated with two parallel line charges can be used to generate on-axis electron vortex beams that can be used to impart a continuously tuneable orbital angular momentum to an electron beam with almost no loss of intensity, apart from the small fraction of the beam that is shielded by the charged wires and their support, thereby demonstrating a clear advantage over all other approaches for creating electron vortex beams. We have also investigated the effect of the length of the wires on Fresnel and Fraunhofer images, as well as a biprism-like effect due to possible charging of the wires. Our simulations have been performed for a setup that can be realised using present-day technology. However, the essential ingredient of the effect is an asymmetric dipole-like line charge distribution, which can be realised in many different ways. Experiments based on the present proposal are in progress.

Acknowledgments

References

[1] D.L. Andrews, M. Babiker, The angular momentum of light, Cambridge University Press, 2012.
[2] J. Verbeeck, G. Guzzinati, L. Clark, R. Juchtmans, R.V. Boxem, H. Tian, A. Béché, A. Lubk, G.V. Tendeloo, Shaping electron beams for the generation of innovative measurements in the (S) TEM, Comptes Rendus Physique 15 (2014) 190–199.
[3] J. Harris, V. Grillo, E. Mafakheri, G.C. Gazzadi, S. Frabboni, R.W. Boyd, E. Karimi, Structured quantum waves, Nature Physics 11 (2015) 629–634.
[4] A. Jesacher, S. Fürhapter, S. Bernet, M. Ritsch-Marte, Shadow effects in spiral phase contrast microscopy, Physical Review Letters 94 (2005) 233902.
[5] S. Bernet, A. Jesacher, S. Fürhapter, C. Maurer, M. Ritsch-Marte, Quantitative imaging of complex samples by spiral phase contrast microscopy, Optics Express 14 (2006) 3792–3805.
[6] S. Fürhapter, A. Jesacher, C. Maurer, S. Bernet, M. Ritsch-Marte, Spiral phase microscopy, in: P.W. Hawkes (Ed.), Advances in Imaging and Electron Physics, volume 146, Elsevier Academic Press, 2007, pp. 1–56.
[7] A.M. Blackburn, J.C. Loudon, Vortex beam production and contrast enhancement from a magnetic spiral phase plate, Ultramicroscopy 136 (2014) 127–143.
[8] M. Uchida, A. Tonomura, Generation of electron beams carrying orbital angular momentum, Nature 464 (2010) 737–739.
[9] J. Verbeeck, H. Tian, P. Schattschneider, Production and application of electron vortex beams, Nature 467 (2010) 301–304.
[10] B.J. McMorran, A. Agrawal, I.M. Anderson, A.A. Herzing, H.J. Lezec, J.J. McClelland, J. Unguris, Electron vortex beams with high quanta of orbital angular momentum, Science 331 (2011) 192–195.
[11] J. Verbeeck, H. Tian, A. Béché, A new way of producing electron vortex probes for STEM, Ultramicroscopy 113 (2012) 83–87.
[12] K. Saitoh, Y. Hasegawa, N. Tanaka, M. Uchida, Production of electron vortex beams carrying large orbital angular momentum using spiral zone plates, Journal of Electron Microscopy 61 (2012) 171–177.
[13] L. Clark, A. Béché, G. Guzzinati, A. Lubk, M. Mazilu, R.V. Boxem, J. Verbeeck, Exploiting lens aberrations to create electron-vortex beams, Physical Review Letters 111 (2013) 064801.
[14] A. Béché, R.V. Boxem, G.V. Tendeloo, J. Verbeeck, Magnetic monopole field exposed by electrons, Nature Physics 10 (2014) 26–29.
[15] Y. Aharonov, D. Bohm, Significance of electromagnetic potentials in the quantum theory, Physical Review 115 (1959) 485–491.
[16] G. Matteucci, G.F. Missiroli, G. Pozzi, A new electrostatic phase-shifting effect, Ultramicroscopy 10 (1982) 247–251.
[17] G. Matteucci, G. Pozzi, New diffraction experiment on the electrostatic Aharonov-Bohm effect, Physical Review Letters 54 (1985) 2469–2472.
[18] G. Matteucci, F. Medina, G. Pozzi, Electron-optical analysis of the electrostatic Aharonov-Bohm effect, Ultramicroscopy 41 (1992) 255–268.
[19] G. Matteucci, G.F. Missiroli, G. Pozzi, P.W. Hawkes, Electron holography of long-range electrostatic fields, in: Advances in Imaging and Electron Physics, volume 122, Elsevier Academic Press, 2002, pp. 173–249.
[20] G. Pozzi, Particles and waves in electron optics and microscopy, in: P.W. Hawkes (Ed.), Advances in Imaging and Electron Physics, volume 194, Elsevier Academic Press, New York, NY, 2016.
[21] A.M. Blackburn, Observation of an electron vortex beam created from a self-charging rod, Microscopy and Microanalysis 22 (S3) (2016) 1710–1711.
[22] A.H. Tavabi, V. Migunov, C. Dwyer, R.E. Dunin-Borkowski, G. Pozzi, Tunable caustic phenomena in electron wavefields, Ultramicroscopy 157 (2015) 57–64.
[23] W.T. Scott, The physics of electricity and magnetism, 2nd Edition, Wiley, New York, 1966.
[24] G. Pozzi, M. Beleggia, T. Kasama, R.E. Dunin-Borkowski, Interferometric methods for mapping static electric and magnetic fields, Comptes Rendus Physique 15 (2014) 126–139.
[25] G. Matteucci, G. Missiroli, E. Nichelatti, A. Migliori, M. Vanzi, G. Pozzi, Electron holography of long-range electric and magnetic fields, Journal of Applied Physics 69 (1991) 1835–1842.
[26] G. Pozzi, Electron holography of long-range electromagnetic fields: A tutorial, in: P.W. Hawkes (Ed.), Advances in Imaging and Electron Physics, volume 123, Elsevier, 2002, pp. 207–223.
[27] K. Keimpema, H. De Raedt, J. De Hosson, Electron holography image simulation of nanoparticles, Journal of Computational and Theoretical Nanoscience 3 (2006) 362–374.
[28] E. Durand, Électrostatique, volume 2, Masson, Paris, 1964.
[29] D.J. Griffiths, Y. Li, Charge density on a conducting needle, American Journal of Physics 64 (1996) 706–714.
[30] M. Born, E. Wolf, Principles of optics: electromagnetic theory of propagation, interference and diffraction of light, 4th Edition, Pergamon Press, Oxford, 1969.
[31] J.W. Goodman, Introduction to Fourier optics, 2nd Edition, McGraw-Hill, New York, 1996.
[32] G. Fursey, Field electron emission from metals, in: I. Brodie, P. Schwoebel (Eds.), Field Emission in Vacuum Microelectronics, Springer, 2005, pp. 1–17.
[33] N. Zouache, A. Lefort, Electrical breakdown of small gaps in vacuum, IEEE Transactions on Dielectrics and Electrical Insulation 4 (1997) 358–364.